



Dose enhancing behavior of hydrothermally grown Eu-doped SnO₂ nanoparticles

R. Sánchez Zeferino, U. Pal, R. Meléndrez, H. A. Durán-Muñoz, and M. Barboza Flores

Citation: [Journal of Applied Physics](#) **113**, 064306 (2013); doi: 10.1063/1.4790486

View online: <http://dx.doi.org/10.1063/1.4790486>

View Table of Contents: <http://scitation.aip.org/content/aip/journal/jap/113/6?ver=pdfcov>

Published by the [AIP Publishing](#)



Re-register for Table of Content Alerts

Create a profile.



Sign up today!



Dose enhancing behavior of hydrothermally grown Eu-doped SnO₂ nanoparticles

R. Sánchez Zeferino,¹ U. Pal,^{1,a)} R. Meléndrez,² H. A. Durán-Muñoz,³
 and M. Barboza Flores²

¹*Instituto de Física, Universidad Autónoma de Puebla, Apdo. Postal J-48, 72570 Puebla, Mexico*

²*Centro de Investigación en Física, Universidad de Sonora, Apartado Postal 5-088, Hermosillo, 83190 Sonora, Mexico*

³*Departamento de Investigación en Polímeros y Materiales, Universidad de Sonora, Apartado Postal 5-088, Hermosillo, 83190 Sonora, Mexico*

(Received 11 November 2012; accepted 22 January 2013; published online 11 February 2013)

Hydrothermally grown SnO₂ and SnO₂:Eu nanoparticles of 4–11 nm size range were analyzed by photoluminescence (PL) and thermoluminescence (TL) spectroscopy to study the effect of Eu-doping on their emission behaviors. It has been observed that most of the incorporated Eu³⁺ ions remain at the interstitial sites of SnO₂ lattice. High Eu-contents in the nanoparticles generate lattice deformation, formation of Eu³⁺/Eu⁰ clusters at interstitial sites, or segregation to their surfaces. Formation of Eu clusters at interstitial sites enhances electronic defect density in the crystal lattice, reorganizes carrier trapping centers, and modifies their activation energies. Room temperature PL emission and beta-irradiated TL dose response of SnO₂ nanoparticles enhance significantly when doped with 0.5 and 1.0 mol. % nominal of Eu³⁺, respectively, opening up their possibilities of applications in bio-imaging and radiation therapy. Possible mechanisms of enhanced PL and TL responses of the samples have been discussed. © 2013 American Institute of Physics.

[<http://dx.doi.org/10.1063/1.4790486>]

I. INTRODUCTION

Intrinsically *n*-type, wide band gap (3.6 eV, at room temperature) semiconductor SnO₂ has been successfully utilized for gas sensing,¹ solar cell fabrication,² as transparent conductive electrode,³ light emitting diode,⁴ and biological imaging.⁵ For biological applications, SnO₂ nanoparticles have been doped with rare-earth (RE) ions like Eu³⁺, Tb³⁺, Er³⁺ to improve their emission efficiency through energy transfer processes between the RE ions and the host lattice.^{6–9} Incorporation of Eu³⁺ ions in SnO₂ has been extensively studied in the literature^{10–13} and it has seen to be most effective for this purpose due to their high stability in oxide matrices and high quantum yield. However, the emission behaviors of Eu³⁺ incorporated metal-oxide nanostructures strongly depend on the location of Eu³⁺ ions in host lattice, which needs a special attention for their biological applications. SnO₂ nanoparticles of 2–100 nm size range have been synthesized utilizing sol-gel,¹⁴ hydrothermal,^{15–17} chemical vapor deposition (CVD),¹⁸ microwave irradiation,¹⁹ and other techniques. Effects of RE ion doping in them have been studied utilizing cathodoluminescence (CL),²⁰ photoluminescence (PL),¹² and other spectroscopic techniques.²¹ However, the mechanism of Eu³⁺ incorporation, specially their location in the host lattice and its effect on the emission behaviors of metal-oxide nanostructures, has not been conclusive.

Nowadays, nanoparticles are of particular importance for biological applications since most of the biological and cellular processes occur at nanoscale. Nanoparticles of different materials are currently under clinical investigation for

utilization as drug-delivery vehicles, contrast agents, and diagnostic devices to get approval by the Food and Drug Administration.²² In medical applications like drug carriers, photothermal agents, contrast agents, and radiosensitizers, the most studied nanostructures include carbon nanotubes, gold nanoparticles, and cadmium selenide quantum dots.²³ Nanoparticles have high concentration of surface atoms and defects at multiple nano-grain boundaries which can create a large number of surface defects like charge-carrier trapping centers at different energy depths. The quantum size effect in nanostructured systems is responsible for luminescence enhancement due to the high probability of radiative electron-hole recombination after exposing them to ionizing and non-ionizing radiations. For radiation detection and dosimetry, novel nanophosphors like CaSO₄:Dy, BaSO₄:Eu, Al₂O₃, ZnO, YAG, LiF:Mg, Cu, P, K₂Ca₂(SO₄)₃:Eu, and Ba_{0.97}Ca_{0.03}SO₄:Eu have been found to be promising in high dose radiation fields due to their characteristic radiation resistance properties.²⁴

Thermally stimulated luminescence, commonly called as thermoluminescence (TL), is the emission of light after thermal stimulation of previously irradiated material. The integrated TL emission response of dosimetric materials is a function of the radiation dose. However, it has been observed that the TL emission intensity of all the above mentioned nanophosphors is lower than their bulk counterparts, while their dose saturation occurs at higher doses in comparison to conventional (bulk) specimen. TL sensitivity and high dose saturation in nanoparticles seem to depend on their size. Though the size effect has been observed very frequently, no clear explanation for the distinct TL characteristics of these nanoparticles is currently available.

^{a)}Electronic mail: upal@sirio.ifuap.buap.mx.

In this communication, we report on the PL and TL studies of hydrothermally grown well crystalline SnO₂ and SnO₂:Eu nanoparticles of uniform sizes to have an idea on the distribution of Eu³⁺ ions and its effects on their emission behaviors. Effects of Eu³⁺ doping at different concentrations on the optical properties of SnO₂ nanoparticles have been studied using diffuse reflectance spectroscopy (DRS) and micro-Raman spectroscopy techniques. Useful properties like photo- and thermally stimulated luminescence enhancement in SnO₂:Eu nanoparticles, which are of extreme importance when dealing with their biomedical applications, are reported and discussed.

II. EXPERIMENTAL

SnO₂:Eu nanoparticles were synthesized using hydrothermal method. In brief, an aqueous solution of NaOH (J. T. Baker, 98.15%) prepared by dissolving 0.75 mol (3.0 g) of NaOH in 30 ml of deionized water was added drop-wise to a 10 ml of SnCl₄•5H₂O (Sigma-Aldrich, 98%) solution containing 0.015 mol (5.25 g) in 10 ml of water under magnetic stirring until the pH of the mixture solution reaches close to 7.0. After 30 min of stirring, 45.0 ml of absolute anhydrous ethanol (J. T. Baker, 99.8%) was added to the mixture. The final pH of the mixture was adjusted to 7.0 by further addition of the NaOH solution. For preparing Eu-doped SnO₂ samples, EuCl₃•XH₂O (Alfa Aesar, 99.9%) of different amounts were added to the reaction mixture under vigorous stirring before adjusting their final pH value. Eu³⁺ ion

contents in the solution were adjusted to maintain their nominal concentrations at 0.5, 1.0, and 2.0 mol. %. The final mixture was homogenized for 10 min and then transferred into a Teflon-lined stainless steel autoclave, which was placed in an oven and heated at 190 °C for 24 h. The resulting white precipitate was centrifuged, washed with water and ethanol several times, and dried at 60 °C for 2 h. Some of the obtained powders were air annealed at 700 °C for 2 h.

Transmission electron microscopic (TEM) observation on the samples was performed in a Philips Tecnai F30 microscope operating at 300 keV after dispersing colloidal samples over carbon coated copper grids and drying at room temperature. Optical properties of the nanoparticles were studied using micro-Raman spectroscopy (Horiba JOBIN-YVON spectrophotometer), room temperature PL, and UV-Vis optical absorption spectroscopy (SHIMADZU UV-3101PC) in the 200–800 nm spectral range. The 325 emission line of a He-Cd laser (Melles Griot) of 15 mW power was utilized for the excitation of the samples. TL glow curves of the samples were recorded using a TL/OSL-DA-20 Risø system equipped with a ⁹⁰Sr/⁹⁰Y beta radiation source (5 Gy min⁻¹). The TL response was measured in between RT and 650 K in nitrogen atmosphere, using a heating rate of 5 °C/s.

III. RESULTS AND DISCUSSION

High resolution TEM (HRTEM) images of the doped and undoped samples (Fig. 1) revealed the formation of

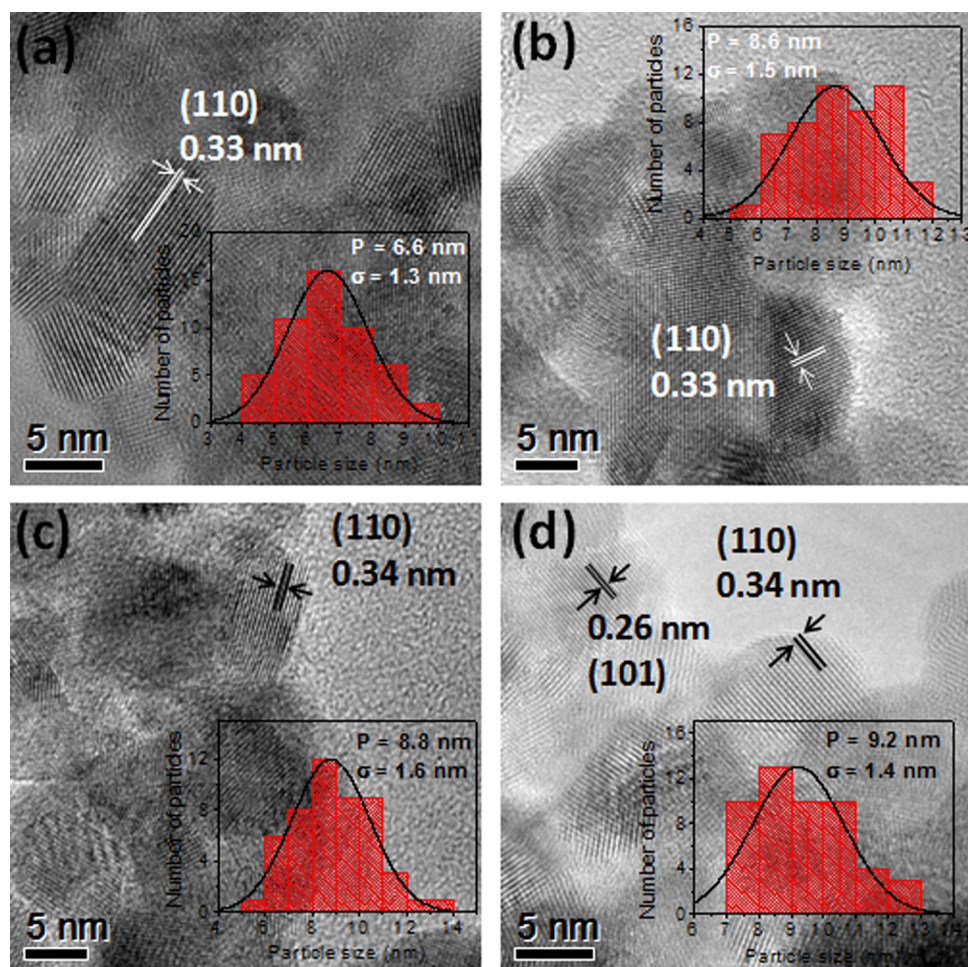


FIG. 1. Typical HRTEM images of SnO₂ nanoparticles doped with (a) 0.0, (b) 0.5, (c) 1.0, and (d) 2.0 mol. % (nominal) of Eu³⁺. Insets show corresponding particle size distribution histograms.

aggregated quasi-spherical nanoparticles in the range of 4–11 nm. It should be noted that no surface modifier or surfactant was utilized in our synthesis. From the size distribution histograms, the average size of the particles was estimated to be 6.6, 8.6, 8.8, and 9.2 nm for the samples doped with 0.0, 0.5, 1.0, and 2.0 mol. % (nominal) of Eu^{3+} , respectively. As we can see, increase in Eu^{3+} content causes a gradual increase in the size of SnO_2 nanoparticles.

The interplanar spacings calculated from the HRTEM images of the undoped sample were 0.33 and 0.26 nm, which correspond to the (110) and (101) lattice planes of rutile SnO_2 , respectively. For the case of 1.0 and 2.0 mol. % Eu^{3+} doped samples, the interplanar spacing of the (110) plane increased to 0.34 nm, probably due to a lattice expansion caused by the incorporation of Eu^{3+} ions in the nanoparticles.

SnO_2 , which crystallizes in tetragonal rutile structure, belongs to the point group D_{4h}^{14} .²⁵ According to group theory, the normal lattice vibrations at the Γ point of the Brillouin zone are as follows:²⁶

$$\Gamma = 1A_{1g} + 1A_{2g} + 1A_{2u} + 1B_{1g} + 1B_{2g} + 2B_{1u} + 1E_g + 3E_u. \quad (1)$$

While the B_{1g} , E_g , A_{1g} , and B_{2g} modes of SnO_2 are Raman active, A_{2u} and E_u are infrared (IR) active, and A_{2g} and B_{1u} are inactive in both Raman and IR.

Raman spectra of all the samples (Fig. 2) revealed three prominent dispersion peaks at about 476, 632, and 777 cm^{-1} , which could be assigned to the E_g , A_{1g} , and B_{2g} fundamental modes of rutile SnO_2 , respectively.²⁷ On the other hand, there appeared two weak Raman peaks located at about 310 and 358 cm^{-1} , which could be associated with the surface modes of SnO_2 nanostructures.²⁸

Furthermore, there appeared a broad dispersion band at about 580 cm^{-1} (S1), which has been reported as the characteristic Raman band of SnO_2 nanostructures by several research groups.^{29,30} The intensity of this particular band has been associated with the size of SnO_2 particles, which generally decreases as the size of the nanoparticles increases. In fact, Patra et al.³¹ have detected a similar Raman peak in between 570 and 577 cm^{-1} for their SnO_2 nanoparticles and nanorods and associated with the surface-related defects in these high surface area nanostructures. In general, the

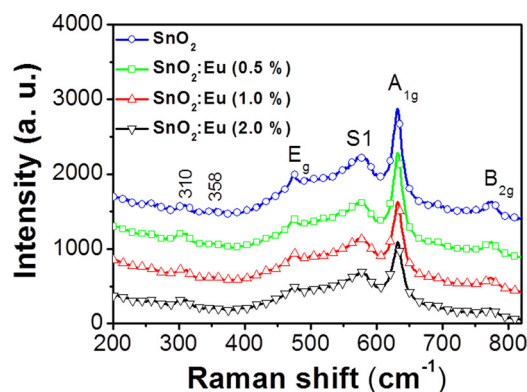


FIG. 2. Raman spectra of SnO_2 and $\text{SnO}_2:\text{Eu}$ nanoparticles annealed at 700 °C.

intensity of all the Raman peaks decreased on increasing the concentration of Eu^{3+} ions. The decrease of peak intensity might be due to the incorporation of structural disorder or a loss of crystallinity of the nanoparticles on incorporating Eu^{3+} ions.

Band gap energies of the doped and undoped samples (Fig. 3) were estimated from their diffuse reflectance spectra utilizing Kubelka-Munk treatment³²

$$\frac{K}{S} = \frac{(1 - R_\infty)^2}{2R_\infty} \equiv F(R_\infty). \quad (2)$$

$F(R_\infty)$ is the so-called remission or Kubelka-Munk function, where $R_\infty = R_{\text{sample}}/R_{\text{reference}}$, K is the absorption coefficient, and S is the scattering coefficient. The band gap energy of the nanoparticles was found to vary in between 3.80 and 3.90 eV with the variation of Eu^{3+} contents. A blue shift of absorption edge was observed on incorporating Eu^{3+} ions in SnO_2 particles. As can be noted, the estimated band gap energy of all the samples is higher than the band gap energy value of bulk SnO_2 (3.6 eV), probably due to the quantum confinement effect of charge carriers in these small particles.

The PL spectrum of the undoped sample (Fig. 4) exhibited weak emission, revealing a broad emission band in 400–800 nm range, with maximum at around 580 nm (inset). This visible emission has been frequently designated as yellow emission (~ 580 nm), assigned to the structural defects such as oxygen vacancies (V_o) and interstitial Sn (Sn_i) in SnO_2 lattice.^{33,34} The PL spectra of all the Eu-doped samples revealed characteristic PL bands associated with the $^5D_0 \rightarrow ^7F_1$ (588–599 nm), $^5D_0 \rightarrow ^7F_2$ (608–633 nm), and $^5D_0 \rightarrow ^7F_3$ (652–661 nm) interband transitions of Eu^{3+} ions along with the weak yellow emission of undoped SnO_2 . While the nanoparticles nominally doped with 0.5 mol. % of Eu^{3+} ions revealed strongest emissions associated with the RE ions, doping at 1.0 mol. % and higher caused a luminescence quenching. However, the extent of PL quenching was not same for all the transitions.

As we know, on irradiating an Eu^{3+} ion doped semiconductor with high energy photons, electrons of its conduction band get excited to the 7F_2 level of the RE ion and then

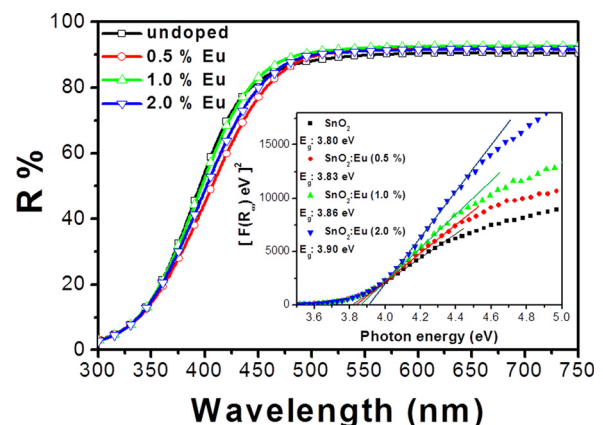


FIG. 3. Diffuse reflectance spectra of the SnO_2 and $\text{SnO}_2:\text{Eu}$ nanoparticles. The inset shows the $[F(R_\infty)]^2$ vs photon energy (Kubelka-Munk) plots of the samples.

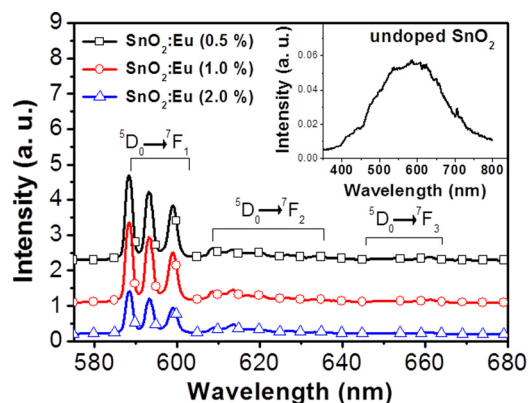


FIG. 4. Room temperature PL spectra of the SnO_2 nanoparticles doped with (a) 0.5, (b) 1.0, and (c) 2.0 mol. % (nominal) of Eu^{3+} ions. The inset shows the PL spectrum of undoped SnO_2 sample.

decay to $^5\text{D}_2$ level ($^7\text{F}_2 \rightarrow ^5\text{D}_2$), and subsequently to the $^5\text{D}_0$ level through nonradiative transition processes. However, photons are emitted for the radiative transitions $^5\text{D}_0 \rightarrow ^7\text{F}_j$ ($J=0, 1, 2, 3, 4$).

As the $^5\text{D}_0 \rightarrow ^7\text{F}_1$ transitions are magnetic dipole allowed, they are not affected by structural changes in the vicinity of Eu^{3+} ions. On the other hand, the $^5\text{D}_0 \rightarrow ^7\text{F}_2$ transitions are electrical dipole allowed ($\Delta J \geq 2$), and very much sensitive to the local crystal field of Eu^{3+} ions. To get an idea of local distribution of Eu^{3+} ions in the SnO_2 lattice, we estimated the intensity ratio of the emissions ($^5\text{D}_0 \rightarrow ^7\text{F}_2 / ^5\text{D}_0 \rightarrow ^7\text{F}_1$) associated with these two transitions, which could be designated as asymmetric ratio.³⁵ An increase in the asymmetric ratio value would mean that most of the Eu^{3+} ions are located at the distorted sites of SnO_2 lattice. On the other hand, a decrease of this ratio would indicate that the Eu^{3+} ions are not located at distorted sites; rather they are segregated to the surface of the SnO_2 nanoparticles. Estimated asymmetric ratios were 0.40, 0.43, and 0.50 for our 0.5, 1.0, and 2.0 mol. % Eu-doped samples, respectively. Such an increase in asymmetric ratio indicates that on increasing the nominal concentration of Eu in the reaction mixture, a higher number of Eu^{3+} ions incorporate into the distorted lattice sites of SnO_2 nanoparticles. As the ionic radius of Eu^{3+} (0.112 nm) is much bigger than the ionic radius of Sn^{4+} (0.071 nm), it is difficult for them to be accommodated at the lattice sites of Sn^{4+} ions of SnO_2 lattice. Therefore, most of the Eu^{3+} ions get incorporated at the interstitial sites of SnO_2 , though a fraction of them could also be segregated to the surface of the nanoparticles. The energy dispersive spectroscopy (EDS) analysis of the samples (Table I) revealed only about 0.09, 0.2, and 0.26 at. % of Eu^{3+} ions in the SnO_2 particles prepared with nominal 0.5, 1.0, and 2.0 mol. % of Eu^{3+} ions in the reaction mixture, respectively. On the other hand, at. % of Sn did not vary significantly on increasing the concentration of Eu. The observations suggest the incorporation of Eu^{3+} ions at interstitial sites, rather than substituting Sn^{4+} ions.

Structural defects in the form of oxygen vacancies (V_o) and interstitial Sn (Sn_i) in the $\text{SnO}_2:\text{Eu}^{3+}$ lattice act as trapping level for electrons and holes. Trapping levels in a semi-conducting system can be investigated by TL spectroscopy,

TABLE I. EDS estimated composition of the SnO_2 and $\text{SnO}_2:\text{Eu}$ nanoparticles after annealing at 700°C .

Sample	Elements (at. %)		
	O	Sn	Eu
SnO_2	80.77	19.23	...
$\text{SnO}_2:\text{Eu}$ (0.5%)	76.47	23.44	0.09
$\text{SnO}_2:\text{Eu}$ (1.0%)	78.27	21.53	0.2
$\text{SnO}_2:\text{Eu}$ (2.0%)	80.86	18.88	0.26

which is a highly sensitive technique to establish the presence and nature of localized states and recombination centers that are responsible for the emission of light after thermal stimulation of a previously irradiated specimen.³⁶

The TL behaviors of the Eu-doped nanoparticles were investigated by measuring their TL response in between RT and 650 K. The TL response of the as-grown nanoparticles was observed to vary from one TL run to another due to the presence of adsorbed water at their surfaces, and a change in their crystallinity during TL measurements. To eliminate these problems, all the samples were air-annealed at 700°C for 2 h before recording their TL glow curves again.

The TL glow curves of the undoped and Eu-doped nanoparticles after irradiating with 1638 Gy of β -rays (Fig. 5) revealed three clear emission bands of varied intensities at about 375, 459, and 580 K. For the 1.0% and 2.0% Eu-doped samples, the position of the TL band near 459 K shifted to

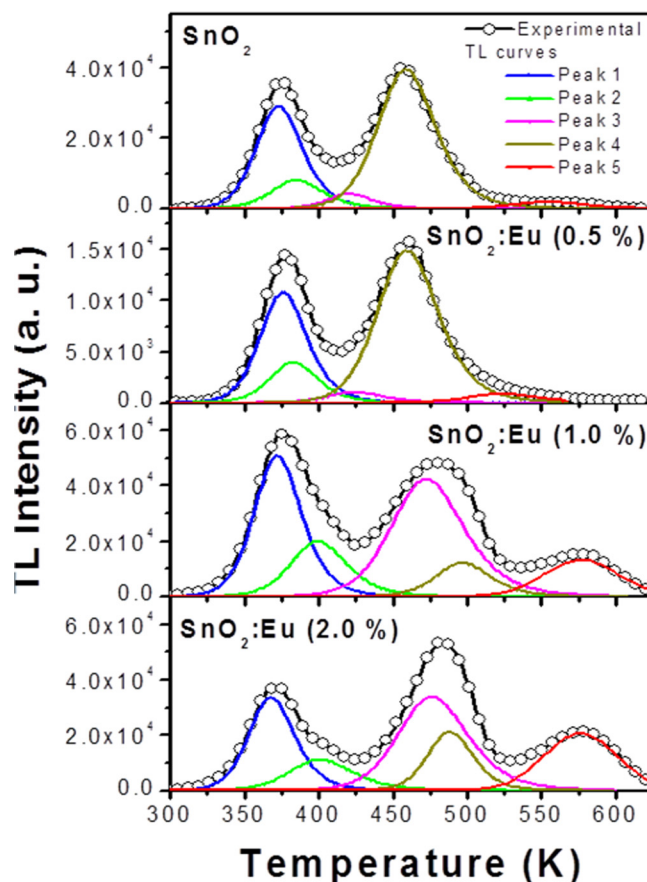


FIG. 5. TL glow curves for the undoped and Eu-doped SnO_2 nanoparticles exposed to 1638 Gy β -radiation and their deconvoluted TL peaks.

higher temperatures (20 and 24 K, respectively), while the intensity of all the emissions varied with the variation of Eu^{3+} ion content. Although the overall intensity of the TL emission increased drastically on incorporating a nominal 1.0% of Eu^{3+} ions, incorporation of Eu^{3+} ions in higher concentrations quenches the TL response of the nanoparticles. Site distortions have significant effects on both PL and TL. Changes in the TL peak temperatures indicate differences in the trapping level energies, perhaps due to lattice expansion and stress caused by dopant incorporation. Therefore, since the TL signals are related to defects, shifts in a glow peak temperature are expected with any alteration in the lattice.

Figure 6 depicts the variation of integrated TL intensity of the samples with irradiation dose. For smaller doses of β -irradiation, integrated TL intensity of all the samples varied quasi-linearly. However, for higher doses (327.6–1638 Gy) of irradiation, the nonlinear behavior of the undoped sample changed to linear one on incorporating Eu^{3+} ions, with no apparent saturation. This linear high-dose response characteristic found in nanophosphors is very different from the characteristics of common bulk dosimetric materials, in which dose saturation is observed at relatively low doses for the case of ionizing and nonionizing radiation.^{24,37}

A careful inspection of the TL glow curve shapes indicates a strong dependence on the Eu^{3+} concentration and of course on the size of $\text{SnO}_2:\text{Eu}$ nanoparticles. We can remember that TEM estimated average particle sizes for the samples doped with 0.0, 0.5, 1.0, and 2.0 mol. % of Eu^{3+} were 6.6, 8.6, 8.8, and 9.2 nm, respectively. As has been stated earlier, the ionic radius of the Eu^{3+} ions is about two times bigger than the ionic radius of Sn^{4+} and most of the Eu^{3+} ions get incorporated at the interstitial sites of SnO_2 causing a strong structural stress as confirmed by the intensity decrease of the 580 cm^{-1} (S1) Raman band of SnO_2 nanoparticle. Therefore, on increasing the concentration of Eu^{3+} ions, in fact we are producing a large number of lattice defects that manifest themselves as a complex set of overlapping TL glow peaks (Fig. 5). In other words, a distorted lattice with high concentration of surface trapping centers and defects at multiple nanograin boundaries may be regarded as the cause for the TL enhancing properties and the widening of the TL glow curve of $\text{SnO}_2:\text{Eu}^{3+}$ nanostructure.

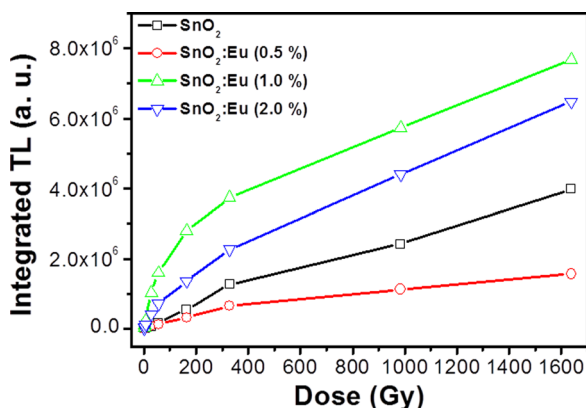


FIG. 6. Variation of integrated TL intensity of the undoped and Eu-doped SnO_2 nanoparticles with β -irradiation dose.

The features displayed in Figs. 5 and 6 are related to the characteristics of $\text{SnO}_2:\text{Eu}^{3+}$ nanostructures. The enhanced TL emission of 1.0% Eu-doped SnO_2 nanoparticles at high-dose ionizing radiation and their improved radiation resistance (high dose saturation) make them attractive for applications in contrast imaging, and radiation detection and monitoring. The physical phenomenon associated with the interaction of radiation with high-Z materials may provide an explanation for the observed properties as suggested by Kortov.³⁷ We can imagine the SnO_2 nanoparticle in a distorted lattice arrangement surrounded by Eu^{3+} interstitial ions. At low Eu^{3+} concentration, the secondary low energy electrons produced by the interaction of the radiation with Eu^{3+} ions interact with the SnO_2 nanoparticles, creating an additional number of charge trappings mainly due to the presence of superficial defects. After thermal stimulation, these trapped charge carriers recombine radiatively giving rise to the observed TL emission. We should recall that undoped SnO_2 nanophosphor is thermoluminescent and the presence of Eu^{3+} ions increases its TL sensitivity due to the generation of secondary electrons triggered by radiation interaction. At higher concentrations of RE ions, the SnO_2 nanoparticles might be surrounded by a great amount of Eu^{3+} ions in such a way that a TL quenching effect occurs due to the formation of a virtual shell of Eu^{3+} which is not thermoluminescent. Therefore, the observed TL enhancing effect is most probably a local dose enhancing radiation effect. If this is so, the great advantage of this phenomenon can be explored in monitoring radiation dose at cellular levels and at the same time providing a way of tracking cellular processes through PL spectral response. The required thermal stimulation may be obtained by other sort of nanomaterials, like well-known metallic nanoshells, which may reach a high intracellular temperature sufficiently enough to trigger TL on a nanoshell $\text{SnO}_2:\text{Eu}^{3+}$ system.

Appearance of bell-shaped broad TL emission bands for the samples (Fig. 5) indicates the presence of a second order TL kinetic process.³⁵ To estimate the depth of the localized trapping levels in the band gap of the samples and their activation energies, we used the glow curve deconvolution (GCD) technique.³⁸ The TL glow curves were fitted with the second-order kinetic equation

$$I(T) = 4I_m \left[e^{\frac{E(T-T_m)}{kT}} \right] \times \left[\frac{T^2}{T_m^2} \left(1 - \frac{2kT}{E} \right) e^{\frac{E(T-T_m)}{kT}} + 1 + \frac{2kT_m}{E} \right]^{-2}, \quad (3)$$

where I_m is the maximum intensity of glow curve and T_m is the corresponding temperature; E (eV) and k (eV K^{-1}) are the activation energy and the Boltzmann constant, respectively.³⁸ In Table II, positions of the TL bands and their estimated activation energies are presented. Five distinct trap levels in the crystalline structure could be detected. Though the incorporation of Eu^{3+} ions did not generate any new trap level in the nanoparticles, for the case of 1.0 mol. % Eu^{3+} doped sample, it causes an increase in TL intensity and shifts trapping levels to higher temperatures (peaks P4 and P5). It should be remarked that a more careful glow curve deconvolution procedure is required to address the fact that the wide

TABLE II. TL peak positions (in absolute temperature, K) and activation energies (in eV) of the carrier trap levels in undoped and Eu-doped SnO₂ nanoparticles.

Sample	Parameters	Peaks				
		P1	P2	P3	P4	P5
SnO ₂	T	372	384	420	458	554
	E	1.09	1.08	1.15	1.25	1.38
SnO ₂ :Eu (0.5%)	T	372	382	424	459	523
	E	1.08	1.01	1.42	1.31	1.58
SnO ₂ :Eu (1.0%)	T	372	399	472	496	576
	E	1.05	1.01	1.10	1.61	1.59
SnO ₂ :Eu (2.0%)	T	368	400	475	488	576
	E	1.01	0.88	1.16	1.92	1.60

TL glow curve is formed by several overlapped TL peaks. Physically, it means that we are in the case of a nanophosphor with a complex continuous trap distribution that may result in successive trapping and detrapping during the excitation and recombination processes. A work on this line is in progress.

As argued earlier, the presence of the Eu³⁺ ions at interstitial sites is probably responsible for the dose enhancing and linear behavior of the SnO₂ nanoparticles as observed in Figs. 5 and 6. Enhanced radiation effects involving interaction of radiation with tissues in contact with high atomic number (Z) materials are well known, but just recently enhancement of radiation effects using high Z nanoparticles like silver, platinum, and gold has been explored.³⁹ As we just mentioned, enhanced radiation effect in our 1.0% Eu-doped SnO₂ nanoparticles is encouraging for their therapeutic applications in biological tissues. On the other hand, enhanced PL emission of lightly doped SnO₂:Eu nanoparticles opens the possibility of their use for biological imaging under UV excitations.

IV. CONCLUSIONS

In summary, incorporation of Eu³⁺ ions in SnO₂ nanoparticles drastically modifies their emission behaviors. Up to a certain concentration, the incorporated Eu³⁺ ions remain at interstitial lattice sites and enhance the characteristic PL emissions of the RE ions. Incorporation of Eu³⁺ ions in higher concentrations probably causes the formation of Eu³⁺/Eu⁰ clusters at the interstitial sites and at the surface of the nanoparticles, quenching their PL emission due to enhanced recombination of photogenerated charge carriers. Incorporated Eu³⁺ ions drastically modify the charge trapping and radiative recombination efficiencies of SnO₂ nanoparticles, producing significant TL and dose enhancing effects for 1.0 mol. % Eu³⁺ doped sample. No apparent dose saturation up to kGy could be observed. The high Z value of Eu and very small sizes of the formed Eu³⁺ or Eu⁰ clusters seem to play main role on the observed TL dose enhancement effect stimulated by the production of low energy secondary electrons through the interaction of the radiation with the high-Z Eu³⁺ ions. Studies are being carried out for different dopants and hosts to verify this effect further. Functionalized nano-

structures with dose enhancing properties are of great importance for applications in radiotherapy, since they allow to deliver a given radiation dose directly to a tumor while preserving its surrounding tissues.

ACKNOWLEDGMENTS

The authors are thankful to VIEP-BUAP (Grant # VIEP/EXC/2012), and CONACyT (Grant # 151767), Mexico for their financial supports.

- ¹J. G. Partridge, M. R. Field, J. L. Peng, A. Sadek, Z. Kalantar-zadeh, J. Du Plessis, and D. G. McCulloch, *Nanotechnology* **19**, 125504 (2008).
- ²K. Hara, T. Horiguchi, T. Kinoshita, K. Sayama, H. Sugihara, and H. Arakawa, *Sol. Energy Mater. Sol. Cells* **64**, 115 (2000).
- ³C. Wang, A. J. Appleby, and F. E. Little, *Solid State Ionics* **147**, 13 (2002).
- ⁴G. Shen, P.-C. Chen, K. M. Ryu, and C. W. Zhou, *J. Mater. Chem.* **19**, 828 (2009).
- ⁵R. R. Gonçalves, M. Ferrari, A. Chiasera, M. Montagna, E. A. Morais, L. V. A. Scalvi, C. V. Santilli, Y. Messaddeq, and S. J. L. Ribeiro, *J. Metastable Nanocryst. Mater.* **14**, 107 (2002).
- ⁶E. E. Nyein, U. Hömmerich, J. Heikenfeld, D. S. Lee, A. J. Steckl, and J. M. Zavada, *Appl. Phys. Lett.* **82**, 1655 (2003).
- ⁷N. Hamelin, P. G. Kik, J. F. Suyver, K. Kikoin, A. Polman, A. Schönecker, and F. W. Saris, *J. Appl. Phys.* **88**, 5381 (2000).
- ⁸M. Nogami, A. Ohno, and H. You, *Phys. Rev. B* **68**, 104204 (2003).
- ⁹M. Nogami, T. Enomoto, and T. Hayakawa, *J. Lumin.* **97**, 147 (2002).
- ¹⁰T. Moon, S.-T. Hwang, D.-R. Jung, D. Son, C. Kim, J. Kim, M. Kang, and B. Park, *J. Phys. Chem. C* **111**, 4164 (2007).
- ¹¹X. Fu, H. Zhang, S. Niu, and Q. Xin, *J. Solid State Chem.* **178**, 603 (2005).
- ¹²A. C. Yanes, J. Del Castillo, M. Torres, J. Peraza, V. D. Rodríguez, and J. Méndez-Ramos, *Appl. Phys. Lett.* **85**, 2343 (2004).
- ¹³P. S. Chowdhury, S. Saha, and A. Patra, *Solid State Commun.* **131**, 785 (2004).
- ¹⁴S. Gnanam and V. Rajendran, *J. Sol-Gel Sci. Technol.* **53**, 555 (2010).
- ¹⁵H. Zhu, D. Yang, G. Yu, H. Zhang, and K. Yao, *Nanotechnology* **17**, 2386 (2006).
- ¹⁶U. Pal, A. C. Pérez, and M. H. Zaldívar, *J. Appl. Phys.* **103**, 064301 (2008).
- ¹⁷U. Pal, M. Pal, and R. S. Zeferino, *J. Nanopart. Res.* **14**, 969 (2012).
- ¹⁸Y. Liu, E. Koep, and M. A. Liu, *Chem. Mater.* **17**, 3997 (2005).
- ¹⁹A. Kar and A. Patra, *J. Phys. Chem. C* **113**, 4375 (2009).
- ²⁰D. F. Crabtree, *J. Phys. D: Appl. Phys.* **7**(1), L17 (1974).
- ²¹H. V. Fajardo, E. Longo, L. F. D. Probst, A. Valentini, N. L. V. Carreño, M. R. Nunes, A. P. Maciel, and E. R. Leite, *Nanoscale Res. Lett.* **3**, 194 (2008).
- ²²B. Y. S. Kim, J. T. Rutka, and W. C. W. Chan, *N. Engl. J. Med.* **363**, 2434 (2010).
- ²³S. Jain, D. G. Hirst, and J. M. O'Sullivan, *Br. J. Radiol.* **85**, 101 (2012).
- ²⁴N. Salah, *Radiat. Phys. Chem.* **80**, 1 (2011).
- ²⁵S. H. Sun, G. W. Meng, G. X. Zhang, T. Gao, B. Y. Geng, L. D. Zhang, and J. Zuo, *Chem. Phys. Lett.* **376**, 103 (2003).
- ²⁶S. P. S. Porto, P. A. Fleury, and T. C. Damen, *Phys. Rev.* **154**, 522 (1967).
- ²⁷P. S. Peercy and B. Morosin, *Phys. Rev. B* **7**, 2779 (1973).
- ²⁸J. Zuo, C. Xu, X. Liu, C. Wang, Y. Hu, and Y. Qian, *J. Appl. Phys.* **75**, 1835 (1994).
- ²⁹W. Chen, D. Ghosh, and S. Chen, *J. Mater. Sci.* **43**, 5291 (2008).
- ³⁰A. Diéguez, A. R. Rodríguez, A. Vilà, and J. R. Morante, *J. Appl. Phys.* **90**, 1550 (2001).
- ³¹A. Kar, S. Kundu, and A. Patra, *J. Phys. Chem. C* **115**, 118 (2011).
- ³²A. E. Morales, E. S. Mora, and U. Pal, *Rev. Mex. Fis. S* **53**, 18 (2007).
- ³³X. Xiang, X. T. Zu, S. Zhu, L. M. Wang, V. Shutthanandan, P. Nachimuthu, and Y. Zhang, *J. Phys. D: Appl. Phys.* **41**, 225102 (2008).
- ³⁴B. Wang, Y. H. Yang, C. X. Wang, N. S. Xu, and G. W. Yang, *J. Appl. Phys.* **98**, 124303 (2005).
- ³⁵R. S. Ningthoujam, V. Sudarsan, and S. K. Kulshreshtha, *J. Lumin.* **127**, 747 (2007).
- ³⁶R. Chen and S. W. S. McKeever, *Theory of Thermoluminescence and Related Phenomena* (World Scientific, Singapore, 1997), p. 3.
- ³⁷V. S. Kortov, *Radiat. Meas.* **45**, 512 (2010).
- ³⁸G. Kitis, J. M. G. Ros, and J. W. N. Tuy, *J. Phys. D: Appl. Phys.* **31**, 2636 (1998).
- ³⁹J. F. Hainfeld, F. A. Dilmanian, Z. Zhong, D. N. Slatkin, J. A. Kalef-Ezra, and H. M. Smilowitz, *Phys. Med. Biol.* **55**, 3045 (2010).